Proceedings of ISFOG 2025
5TH INTERNATIONAL SYMPOSIUM ON
FRONTIERS IN OFFSHORE GEOTECHNICS
Nantes, France | June 9-13 2025

ISBN 978-2-85782-758-0

Review of methods for soil damping estimation for +15 MW offshore wind turbines supported on monopile foundations

N. C. Dahl*
Wood Thilsted, Copenhagen, Denmark

M. B. Nielsen
Wood Thilsted, Copenhagen, Denmark

I. A. Richards
Wood Thilsted, London, United Kingdom

ncd@woodthilsted.com

ABSTRACT: This paper reviews different methods for the calculation of soil damping for monopile structures supporting +15 MW offshore wind turbines. Accurate damping calculation is essential for accurate calculation of fatigue damage accumulation, and with up to 60% of the fatigue damage coming from the stand-still period where the soil damping is the largest contributor to the inherent structural damping, accurate soil damping calculation is crucial for monopile design. Using a publicly available soil profile and a generic yet realistic monopile design, this paper demonstrates the range of soil damping obtained from different soil damping methods being between 0.13 to 7.69%. This paper investigates why there are such significant variations in the soil damping values calculated using different methods, considering the contribution of stored energy in the monopile, the applied strain-displacement relationships and other modelling assumptions. Given the large variation in calculated soil damping values, it is crucial to have a reliable soil damping method validated using full-scale measurements. Such measurements are, however, not available for the current size of monopiles supporting the latest turbines, and the significantly varying soil damping results highlight the need for such data.

Keywords: Damping; soil damping; Offshore wind turbines; Monopile; Soil-structure interaction.

1 INTRODUCTION

As offshore wind turbine generators (WTGs) grow in size, so do their foundations and the associated design challenges. For WTGs supported on monopile (MP) foundations, a key aspect is the calculation of soil damping, as it has a direct effect on the fatigue damage and, thus, the lifetime of the structure.

Damping of WTGs comes from various sources, such as aerodynamic damping, inherent material (steel) damping, hydrodynamic damping and soil damping. Active damping devices may also be used.

Aerodynamic damping, which arises from the interaction between the blades and the wind, provides the largest contribution to overall damping. Aerodynamic damping is most pronounced in the fore-aft direction (perpendicular to the rotor plane), while its impact in the side-side direction is relatively limited. Furthermore, during the typical downtime of 5–8% of a WTG's operational lifetime, aerodynamic damping is significantly reduced. In this stand-still period as well as cases with loading in the side-side direction, soil damping provides a significant fraction of the total damping and is thus important to estimate precisely. Despite the stand-still period being only approximately 5-8%, up to 60% of the total fatigue damage can be accumulated during this period.

In fatigue calculations, damping plays a significant role, particularly under resonant loading, where it has a direct linear relationship with the reduction of fatigue-induced damage. Reduced damping can thus result in a substantial increase in steel required in the MP or a reduced lifetime.

There is no common or standard method for calculating soil damping for MPs, and available methods yield significantly varying results. The most commonly used methods for calculating the various foundation damping contributions date back to the early eighties (Cook and Vandiver, 1982), where they were developed for slender piles supporting multi-legged platforms rather than the large-diameter MPs supporting the +15 MW WTGs being installed today. Two recent papers by Zhang et al. (2021) and Stuyts et al. (2022) suggest alternative soil damping calculation methods, but both emphasise the lack of field measurement data for validation of the methods.

In particular, no data is available for +15 MW WTGs. The importance of accurately calculating soil damping has intensified with the increasing size of WTGs, as a smaller proportion of the overall structure is embedded in the soil, limiting the potential for energy dissipation and, consequently, soil damping. A comprehensive review of foundation damping can be found in Malekjafarian et al. (2021), however, both the WTG and MP size in focus are smaller than the structures being designed today. Furthermore, the methods and results pre-date the publication of PISA soil reaction curves (Burd et al., 2020 and Byrne et al., 2020) which causes the analysed piles to have a larger penetration than current MPs.

This paper presents and compares results using different soil damping methods from Cook & Vandiver, Zhang and Stuyts and investigates and explains the differences in the results.

2 MODELLING SOIL DAMPING

The methods presented by Cook & Vandiver, Zhang and Stuyts all calculate soil damping, ζ_{soil} (-), within a 1D-Winkler spring model at a specified displacement level, applying hysteresis damping and calculating stored and dissipated energy components. The soil damping investigated in this paper is thus the hysteretic soil damping, i.e. material soil damping. Another source of soil damping is from the radiation of waves in the soil volume surrounding the MP. This radiation damping is, however, neglected as the frequency at which such damping occurs exceeds the vibrational frequencies of MP-supported WTGs during standard loading (Cook and Vandiver, 1982).

Damping is throughout this paper represented as the ratio of critical damping, ζ.

2.1 Pile-soil model

To calculate the soil damping and model the structure, the structure is discretised into elements with each node denoted i (-) and with a total number of N (-) nodes. The soil is modelled using 1D-Winkler springs, e.g. *p-y* springs, at each pile node, as illustrated in Figure 1, which also defines the vertical coordinate, z (m).

2.2 Soil displacements

Specification of the MP displacement, u (m), to apply in soil damping calculation is crucial, as the more the MP moves, the greater the strains in the soil, and the more soil damping will be obtained. However, this choice is left to the MP designer as no clear guidelines exist.

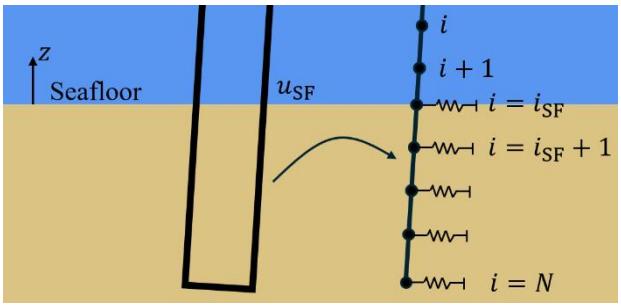

Figure 1. Pile model description.

Typically, a representative seafloor (SF) displacement, u_{SF} (m), is defined, from which the displacement down the pile is obtained by a static displacement-controlled analysis or based on the lateral modal displacements of the first bending mode of the structure. The displacement at the hub-height (HH) of the WTG can be obtained from the same approach.

The dynamic response of an MP-supported WTG subject to wind and wave loads is primarily dominated by the first bending mode; consequently, all soil damping is assumed to originate from this. Higher modes do contribute to the response to transient events such as turbine shutdowns, ship impacts, ice, and seismic loading; however, these cases are not considered further here.

To define the representative SF displacement, load cases where soil damping has a significant impact are most suitable. As mentioned, these are at WTG stand-still and where the loading frequency, ω_{load} (rad/s), is close to the first natural frequency of the structure, ω_{nat} (rad/s), i.e. at resonance. Figure 2 shows how the influence of damping on the dynamic amplification factor (DAF) increases close to resonance.

2.3 Soil material damping curves

Soil material damping curves relate shear strain in the soil, γ (-), to soil material damping, β_s (-), and are a key input to damping calculations. A soil material damping curve comes in pair with a shear modulus degradation curve, describing the decrease in shear modulus, G (Pa), as a function of γ. The necessary lab tests to obtain such curves are most often resonant column tests, cyclic direct simple shear tests or a

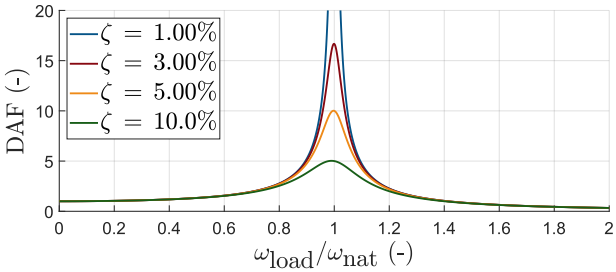

Figure 2. The influence of damping on the dynamic amplification factor (DAF).

combination of the two as they represent different shear strain levels. Where insufficient laboratory data is available to derive these curves, the curves found in DNV-RP-C212 (2021) may be applied.

2.4 Hysteresis damping

All methods presented in this paper calculate soil damping based on hysteresis damping, where the damping ratio, ζ_{Hys} (-), is equal to the ratio between the dissipated energy of a single load cycle, ΔE (J), and the total energy stored in the system during that load cycle, E (J), see e.g. Malekjafarian et al. (2021), illustrated in Figure 3 in terms of force, F (N), and displacement, x (m), and defined as:

$$\zeta_{\mathrm{Hys}} = \frac{1}{4\pi}\frac{\Delta E}{E} \tag{1}$$

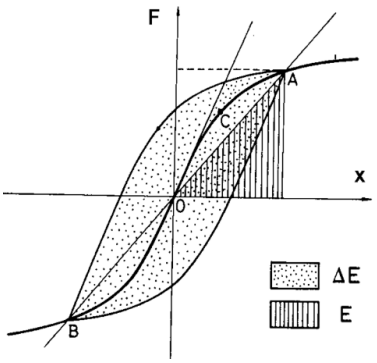

Figure 3. Definition of hysteresis damping Malekjafarian et al. (2021).

For a discretised model with N nodes, damping can be calculated as:

$$\zeta_{\mathrm{soil}} = \frac{1}{4\pi}\frac{\sum_{i=1}^{N}\Delta E_i(z_i,u_i,\gamma_i)}{\sum_{i=1}^{N}E_i(z_i,u_i,\gamma_i)} \tag{2}$$

where ΔE_i is calculated as follows, see e.g. Cook and Vandiver (1982):

$$\Delta E_i(z_i,u_i,\gamma_i) = 4\pi\,\beta_{\mathrm{s},i}(z_i,\gamma_i)\,E_{\mathrm{soil},i}(z_i,u_i,\gamma_i) \tag{3}$$

where $E_{\mathrm{soil},i}$ (J) is the stored elastic energy in the i^{th} soil spring. The different soil damping methods are differentiated by the approach for the calculation of $E_{\mathrm{soil},i}$ and E_i.

2.5 Soil damping methods

2.5.1 Cook & Vandiver

This method (Cook and Vandiver, 1982) (CV) derives the soil damping from each bending mode of the structure and was developed for long and slender piles supporting offshore platforms and validated using data from a pile with diameter, D (m), of $D = 2.13$ m in the Gulf of Mexico. This method calculates $E_{\mathrm{soil},i}$ from the *p-y* curves:

$$E_{\mathrm{soil,CV},i}(z_i,u_{\mathrm{CV},i}) = \frac{1}{2}k_{\mathrm{s},i}(z_i,u_{\mathrm{CV},i})\left(u_{\mathrm{CV},i}\,(z_i)\right)^2 \tag{4}$$

where $k_{\mathrm{s,i}}$ (N/m) is the soil spring secant stiffness at the mobilised point of the *p-y* curve at the i^{th} soil spring and $u_{\mathrm{CV},i}$ (m) is calculated assuming that mode 1 is the only contributing mode to the soil damping utilising:

$$u_{\mathrm{CV},i}(z_i) = u_{\mathrm{HH}}\,\Phi_{1,i}(z_i) \tag{5}$$

where $\Phi_{1,i}$ (-) is the lateral modal displacement for mode 1 at the i^{th} node normalised to 1 at HH and u_{HH} (m) is the displacement at HH obtained as described in Section 2.2.

The method calculates E for the whole structure, rather than summing over N nodes:

$$E_{\mathrm{CV}} = \frac{1}{2}m_1\,\omega_1^2\,u_{\mathrm{HH}}^2 \tag{6}$$

where the modal stiffness is represented by m_1 (kg) and ω_1 (rad/s) being the modal mass and natural frequency associated with mode 1, respectively. Inserting (3), (4) and (6) into (1) yields the following expression for the soil damping:

$$\zeta_{\mathrm{soil,CV}} = \frac{1}{m_1\omega_1^2}\sum_{i=i_{\mathrm{SF}}}^{N}\beta_{\mathrm{s},i}(z_i,\gamma_i)\,k_{\mathrm{s},i}(z_i,u_i)\,\Phi_{1,i}(z_i)^2 \tag{7}$$

The original paper assumes that the material soil damping is constant and in the range of 3-10%. However, this soil damping method has been adopted by industry and refined to use strain-dependent material soil damping, $\beta_{\mathrm{s},i}$. In this paper, the shear strain relationship presented in the Stuyts method and described in Section 2.5.3 is applied in combination with the Cook & Vandiver soil damping method.

2.5.2 Zhang et al.

This method (Zhang et al., 2021) (Z) is validated by a 3D finite element (FE) model with a pile with $D = 2.14$ m. Clay conditions with an over-consolidation ratio of 1 and a plasticity index of 60% are applied. The soil damping method described here is approach 2 presented in the paper, which models the soil-pile interaction as lumped springs and dashpots at the SF. The method uses (2) to obtain $\zeta_{\mathrm{soil,Z}}$ and $E_{\mathrm{soil},i}$ is calculated from the *p-y* curves:

$$E_{\mathrm{soil,Z},i}(z_i, u_i) = \frac{1}{2}\, p_i(z_i, u_i)\, u_i(z_i) \qquad (8)$$

where p_i (N) is the mobilised soil reaction from the i^{th} p-y curve at u_i, hence $E_{\mathrm{soil,Z},i} = E_{\mathrm{soil,CV},i}$ when the same p-y curves are applied. The method calculates E_i as the sum of the stored elastic energy in the soil springs, $E_{\mathrm{soil,Z},i}$, and the pile elements, $E_{\mathrm{pile,Z},i}$ (J):

$$E_{\mathrm{Z},i}(z_i) = E_{\mathrm{soil,Z},i} + E_{\mathrm{pile,Z},i} \qquad (9)$$

$$E_{\mathrm{pile,Z},i}(z_i) = \frac{1}{2} M_i(z_i) \Delta\theta_i(z_i) \qquad (10)$$

where M_i (Nm) is the bending moment and $\Delta\theta_i$ (-) is the change in pile rotation in the i^{th} pile element generated from u_i. The Zhang method indicates that only the stored energy in the embedded part of the MP should be considered. However, this neglects the stored energy for the MP above the SF. In this paper, the stored energy of the full structure, i.e. including nodes above the SF, is considered. To obtain $\beta_{\mathrm{s},i}$ the following shear strain relationship is applied:

$$\gamma_{\mathrm{Z},i}(z_i, u_i) = \frac{1}{3.6\, D_i(z_i)}\, u_i(z_i) \qquad (11)$$

This relation is derived from 3D-FE analyses which models plane-strain conditions, representative for a flow-around failure mechanism.

2.5.3 Stuyts et al.

This method (Stuyts et al., 2022) applies a relationship between strain and displacement presented by Kagawa and Kraft (1980) and compares results to damping measurements from piles with $D = 7$ to 8 m in layered soil profiles with stiff overconsolidated clays and dense sands. This method also uses (2) to obtain $\zeta_{\mathrm{soil,S}}$ and it calculates $E_{\mathrm{soil},i}$ from shear modulus degradation curves as follows:

$$E_{\mathrm{soil,S},i}(z_i, u_i, \gamma_i) = \frac{1}{2}\, G_i(z_i, \gamma_i)\, \gamma_i(z_i, u_i)^2 \qquad (12)$$

In the Stuyts method, $E_{\mathrm{soil,S},i}$ is also used directly as E_i giving:

$$E_{\mathrm{S},i}(z_i, u_i, \gamma_i) = E_{\mathrm{soil,S},i}(z_i, u_i, \gamma_i) \qquad (13)$$

The Stuyts method uses the following relation to obtain γ for calculation of $\beta_{\mathrm{s},i}$ and G_i:

$$\gamma_{\mathrm{S},i}(z_i, u_i) = \frac{1+\nu_i}{2.5\, D_i(z_i)}\, u_i(z_i) \qquad (14)$$

where ν_i (-) is Poisson's ratio of the soil at the i^{th} soil spring. For undrained conditions, thus $\nu = 0.5$, the Stuyts shear strain relation (14) yields shear strains that are 2.16 times larger than the Zhang shear strain relation (11).

3 EXAMPLE APPLICATION

To illustrate the results of the different soil damping methods, both a soil profile and an MP design are required. The soil profile is taken from the publicly available geotechnical interpretative report from the wind farm Ijmuiden Ver in the Dutch part of the North Sea (Fugro, 2023). The design profile denoted IJV001 has been selected, and the so-called '*k1*' values have been applied. Figure 4 illustrates the geotechnical parameter values and shows that the applied water depth is 30 m. Poisson's ratio for the soil is set to 0.5 as it is assumed that for dynamic cyclic loading, which is the source of the soil damping, the soil

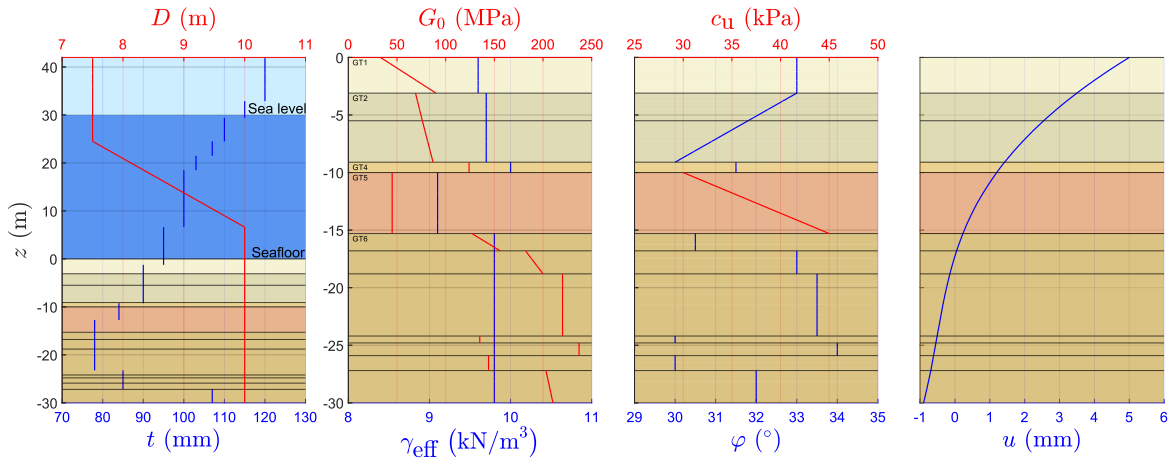

Figure 4. Input parameters for the soil damping calculations: Wall thickness, t (m), and pile diameter, D (m), for the MP. The effective unit weight, γ_{eff} (N/m^3), the initial shear modulus, G_0 (Pa), the friction angle, φ (°), and the undrained shear strength, c_u (Pa), for the soil profile. Displacement, u (m), for the embedded MP.

behaves according to undrained continuum mechanics.

The applied soil reaction curves are the PISA curves both for sand (Burd et al., 2020) and clay (Byrne et al., 2020) without any additional adjustment or calibration. Zhang et al. describe several different *p-y* curves, including scaled, unscaled, cyclic, and FE-derived *p-y* curves, however, it is ambiguous which to apply. In this paper, the same *p-y* curves are applied for all damping methods. The soil material damping curves applied in the soil damping calculations are the relevant curves from DNV-RP-C212 (2021) here being the middle curve for sands and the curve with a plasticity index of 30% for clays.

The example MP supports a 15 MW turbine with a HH of 136 m above sea level. The MP design is illustrated in Figure 4 both in terms of wall thickness, t (m), and D. The design is a simplified version of the design generated by Wood Thilsted's internal MP design tool, Morpheus. Morpheus is an MP design software that solves the structural model consisting of 2D Timoshenko beam elements supported by Winkler springs as described in Nielsen et al. (2022).

Finally, u is also illustrated in Figure 4 where $u_{SF} = 5$ mm has been adopted based on experience gained from several North Sea offshore wind projects.

4 RESULTS & DISCUSSION

Table 1 presents soil damping values calculated with the described methods, while Figure 5 shows intermediate results. The soil damping results are seen to vary greatly with the different methods.

Table 1. Soil damping from the different methods in percent of critical damping.

$\zeta_{soil,CV}$	$\zeta_{soil,Z}$	$\zeta_{soil,S}$
0.13%	0.17%	7.69%

The main differences in the methods leading to this large variation are the inclusion of the energy stored in the pile and the γ-relation. This is proved by modifying the Zhang method using the assumptions of the Stuyts method. First, the pile energy is omitted in the Zhang method to derive $\zeta_{soil,Z,p}$. Then, the γ-relation from the Zhang method, derived from an FE-model, is replaced by the one in the Stuyts method, being a widely used formulation included in the *p-y* curves for clay (DNV-RP-C212, 2021). This derives $\zeta_{soil,Z,\gamma}$. Lastly, both modifications are applied deriving $\zeta_{soil,Z,p,\gamma}$. All three alternative soil damping values are presented in Table 2.

Table 2. Soil damping from the Zhang method with modifications. Soil damping from the Zhang and Stuyts method from Table 1 is added for comparison.

$\zeta_{soil,Z,p}$	$\zeta_{soil,Z,\gamma}$	$\zeta_{soil,Z,p,\gamma}$	$\zeta_{soil,Z}$	$\zeta_{soil,S}$
5.18%	0.24%	7.43%	0.17%	7.69%

Table 2 shows how crucial both the pile energy and the γ-relation are. Omitting the pile energy from the Zhang method yields a soil damping more than 29 times larger than the original soil damping, while changing the γ-relation leads to a 41% increase.

When deriving the soil damping that will be applied in the global model, containing both WTG and MP, it is necessary to relate the dissipated energy in the soil to the energy stored in the global system. This is only done by including all the energy stored in the global model, which includes the pile energy in the full structure. This is the case in the Cook & Vandiver method and is also ensured in the Zhang method presented in this paper.

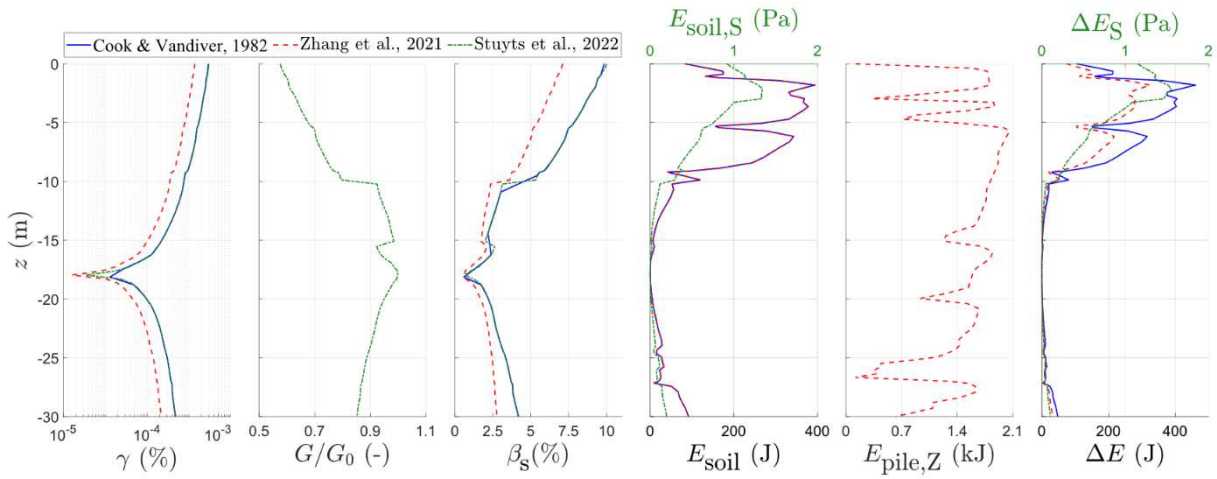

Figure 5. Intermediate results applying the soil damping methods.

Another crucial design aspect is the choice of *p-y* curves to apply. This is not only crucial for the general MP response, and thus for u_{SF} and Φ_1, but is especially important in the Cook & Vandiver and Zhang method, where the curves are applied directly in the soil damping calculation. The softer the curves, the more the MP displaces, and the more soil damping is obtained. However, stiffer curves are beneficial for many other aspects of MP design, and designers generally seek to maximise stiffness. Hence, this aspect should be considered carefully.

Soil damping can also be calculated directly from the global response of the MP. This requires a well-calibrated 3D-FE model which will inherently capture the full soil-structure interaction and thus not be limited to modelling only the lateral *p-y* curve reactions as in the presented methods. This approach is thus likely to provide higher soil damping as the model can inherently account for more dissipation in the soil, e.g. due to shear at the pile-soil interface. The REDWIN foundation model (Page et al., 2019) takes this type of approach, where the hysteretic response, and therefore damping, is modelled using a suitably calibrated multi-surface kinematic hardening model, formulated as a macro-element, which aligns with the Masing rules (Masing, 1926).

All presented soil damping methods have limitations regarding application in MP design for +15 MW WTGs, which also highlights the need for full-scale measurements for validation. In short, the Cook & Vandiver method is derived for piles with significantly different geometries; the Zhang method assumes soil failure in a plane strain flow-around mechanism, which is not applicable to large-diameter MP; and the Stuyts method is validated for a displacement level significantly smaller than the one applied in the paper and it does not include the energy stored in the pile.

5 CONCLUSIONS

From calculating the soil damping from the different presented methods, it can be concluded that the range of results is significant. Several limitations and differences between the methods are the cause of this, with the most significant ones being discrepancies in which and how the energy contributions are calculated. This is demonstrated by the similarity of the results using different methods when the key assumptions on pile energy and γ-relationship are aligned. The results highlight how crucial full-scale measurements are to obtain reliable damping estimates, which is a challenge across the whole offshore wind industry. Sharing of data for +15 MW turbines by offshore wind turbine operators would thus be of high value and contribute to avoiding both under- and over-estimation of damping, which in both cases have significant consequences for the structural design.

AUTHOR CONTRIBUTION STATEMENT

N. C. Dahl: Conceptualization, Data curation, Formal Analysis, Investigation, Methodology, Software, Visualization, Writing - Original draft. **M. B. Nielsen**: Conceptualization, Methodology, Supervision, Writing - Reviewing and Editing. **I. A. Richards**: Conceptualization, Methodology, Supervision, Writing - Reviewing and Editing.

REFERENCES

Burd, H., Taborda, D. M. G., Zdravkovic, L., Abadie, C., Byrne, B., Houlsby, G., Gavin, K., Igoe, D., Jardine, R., Martin, C., Mcadam, R., Pedro, A. and Potts, D. (2020) PISA design model for monopiles for offshore wind turbines: application to a marine sand, *Géotechnique*, Vol. 70, pp. 1048-1066.

Byrne, B., Houlsby, G., Burd, H., Gavin, K., Igoe, D., Jardine, R., Martin, C., Mcadam, R., Potts, D., Taborda, D. M. G. and Zdravkovic, L. (2020) PISA design model for monopiles for offshore wind turbines: application to a stiff glacial clay till, *Géotechnique*, Vol. 70, pp. 1030-1047.

Cook, M. and Vandiver, J. K. (1982) Measured and predicted dynamic response of a single pile platform to random wave excitation. In: *Proceedings of the 14th annual Offshore Technological Conference*, Houston, United States of America.

DNV (2021) DNV-RP-C212 Offshore soil mechanics and geotechnical engineering.

Fugro (2023) IJmuiden Ver Wind Farm Zone – Sites I-IV Geotechnical Interpretative Report Final Interim, Netherlands Enterprise Agency, The Netherlands.

Kagawa, T. and Kraft, L. M. (1980) Lateral load-deflection relationships of piles subjected to dynamic loadings, *Soils and foundations*, Vol. 20 (4), pp. 19-36.

Malekjafarian, A., Jalilvand, S., Doherty, P. and Igoe, D. (2021) Foundation damping for monopile supported offshore wind turbines: A review. *Marine Structures*, Vol. 77, pp. 102937.

Masing, G. (1926) Eigenspannumyen und verfeshungung beim messing. In: *Proceedings of Second International Congress of Applied Mechanics*, Zurich, Switzerland.

Nielsen, M. B., Hindhede, D., Palmer, M. and Thilsted, C. L. (2022) A highly efficient and rapid cost-optimization framework for offshore wind turbine foundations for an entire windfarm site, In: *Proceedings of ASME 2022 International Offshore Wind Technical Conference*, Boston, United States of America.

Page, A., Norén-Cosgriff, K., Skau, K. and Kaynia, A. (2019) REDWIN Foundation Models for Integrated Dynamic Analyses of Offshore Wind Turbines, In: *Proceedings of the ASME 2019 38th International Conference on Ocean, Offshore and Arctic Engineering*, Glasgow, Scotland.

Stuyts, B., Weijtjens, W. and Devriendt, C. (2022) Revised soil damping using realistic pile-soil interaction models. In: *Proceedings of the 2nd Vietnam Symposium on Advances in Offshore Engineering*, Ho Chi Minh City, Vietnam, pp. 441-448.

Zhang, Y., Aamodt, K. and Kaynia, A. (2021) Hysteretic damping model for laterally loaded piles. *Marine Structures,* Vol. 76, pp. 102896.